Electronic Supplementary Material (ESI) for Inorganic Chemistry Frontiers.
This journal is © the Partner Organisations 2021

-Supplementary Information -

Triiron clusters derived from dinuclear complexes related to the active site of [Fe-Fe] hydrogenases: Steric effect of the dithiolate bridge on redox properties, a DFT analysis.

Ahmad Hobballah,[a] Federica Arrigoni,*, [c] Catherine Elleouet,*, [a] Claudio Greco,*, [b] Maxime Laurans,[a] François Y. Pétillon,[a] Philippe Schollhammer,*,[a]

a UMR CNRS 6521, Université de Bretagne Occidentale, Brest, France.

b Department of Earth and Environmental Sciences University of Milan-Bicocca, Piazza della Scienza, 1, 20126 Milan, Italy.

c Department of Biotechnology and Biosciences, University of Milan-Bicocca, Piazza della Scienza, 2, 20126 Milan, Italy

Figure S21. Cyclic voltammetry of $[Fe_3(CO)_5(\kappa^2\text{-dppe})(\mu\text{-pdt}^{Et2})(\mu\text{-pdt})]$ (**2**) (C = 1.20 mM) in presence of CF_3SO_3H in CH_2Cl_2-$[NBu_4][PF_6]$ 0.2 M at v = 0.2 V s^{-1} under Ar .

Figure S22. Cyclic voltammetry of **4** (2.2 mM) in presence of CH_3SO_3H (left) and CF_3SO_3H (right) in CH_2Cl_2-$[NBu_4][PF_6]$ 0.2 M.

Table S1. IR and $^{31}P\{^{1}H\}$ spectroscopic data for **6-7**.

Complex	IR (CH_2Cl_2, cm^{-1}), $\bar{\upsilon}$(CO)	$^{31}P\{^{1}H\}$ NMR ($CDCl_3$, δ : ppm)
6	2044 (m), 1981 (s), 1960 (w), 1919 (w)	61.6 (s)
7	2041 (m), 1983 (s), 1962 (w), 1921 (w)	61.9 (s)

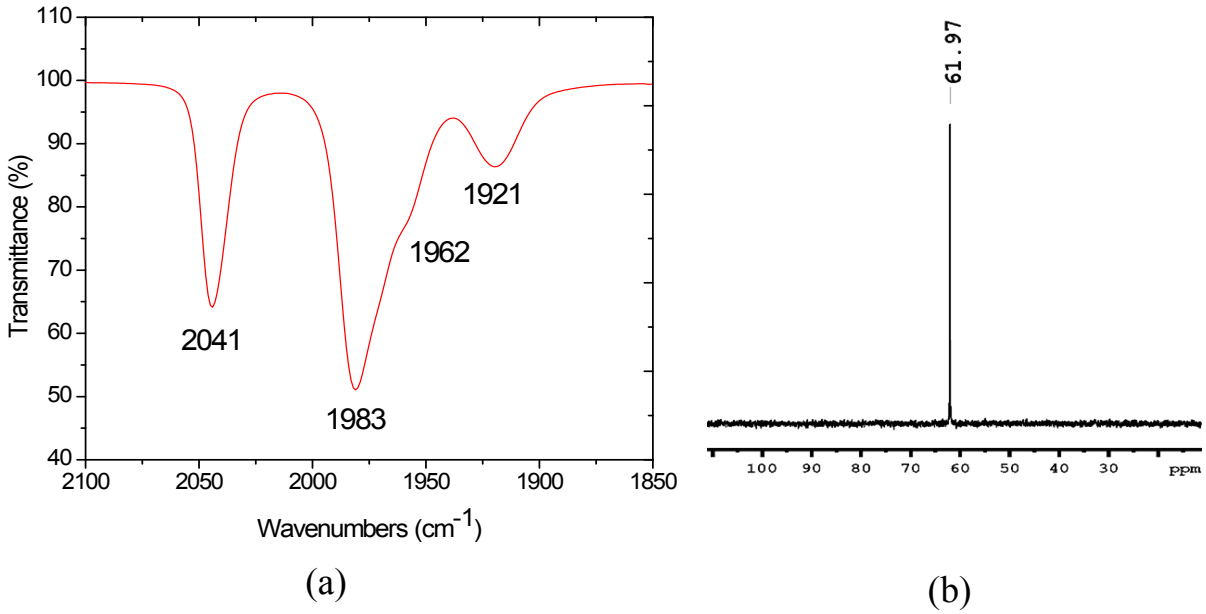

Figure S1. a) IR (CH_2Cl_2), b) $^{31}P\{^{1}H\}$ NMR ($CDCl_3$) spectra of **6** at 25°C.

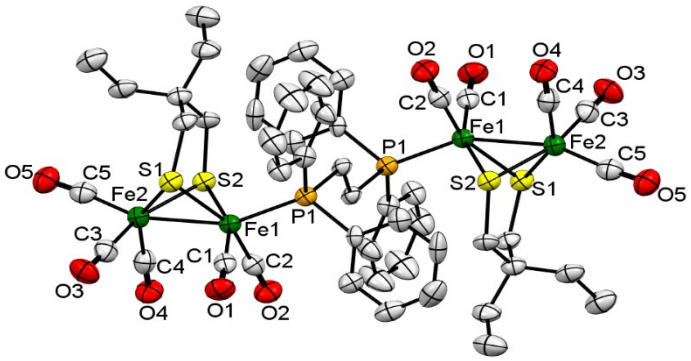

Figure S2. ORTEP view of [{$Fe_2(CO)_5(\mu$-$pdt^{Et2})$}$_2(\mu$-dppe)] (**6**)

Table S2. Selected distances for **6**.

		6
Distance (Å)	Fe1-Fe2	2.5079(14)
	Fe1-S1	2.2748(18)
	Fe1-S2	2.2738(17)
	Fe2-S1	2.277(2)
	Fe2-S2	2.2685(19)
	Fe1-P1	2.220(2)
Angles (°)	Fe2-Fe1-P1	153.61(6)
	C5-Fe2-Fe1	158.0(2)
	Fe1-S1-Fe2	66.87(6)
	Fe1-S2-Fe2	67.03(5)

Table S3. Crystallographic data of [{$Fe_2(CO)_5$(μ-pdt^{Et2})}$_2$(μ-dppe)] (**6**)

	6
Empirical formula	$C_{50}H_{52}Fe_4O_{10}P_2S_4$
Formula weight	1226.50
Temperature/ K	150(2)
Wavelength/Å	0.71073
Crystal system	Triclinic
Space group	P -1
a (Å)	11.0392(9)
b (Å)	11.3968(10)
c (Å)	11.9267(11)
α (°)	110.934(8)
β (°)	94.419(7)
γ (°)	110.140(8)
V (Å^3)	1281.07(19)
Z	1
ρ_{calcd} (Mg/mm^3)	1.590
μ (mm^{-1})	1.393
F(000)	630
Crystal size (mm)	0.13 x 0.05 x 0.03
Crystal color	Red
Crystal shape	Rounded plate // (0 0 1)
Range of θ (°)	3.47 to 26.37
Limiting indices	$-13 \le h \le 13$, $-14 \le k \le 13$, $-14 \le l \le 11$
Reflections collected/unique	8861 / 5210
R_{int}	0.0918
Completeness to θ= 26.37	99.8 %
Absorption correction	Analytical
Max. / Min. Transmission	0.9594 / 0.8397
Refinement method	Full-matrix least-squares on F^2
Data /Restraints /Parameters	5210 / 0 / 318
R_1 [I>2σ(I)]	0.0723
wR_2 [I>2σ(I)]	0.1102
R_1 (all data)	0.1403
wR_2 (all data)	0.1417
Goodness of fit on F^2	0.948
$\Delta\rho_{max}$, $\Delta\rho_{min}$ [e.Å^{-3}]	0.771, -0.666

Table S4: Selected Bond (Å) and angles (°) for complexes **1**, **2** and **3**, theory vs. experiment

		Complex **1***		Complex **2**		Complex **3**	
		Experiment	Theory	Experiment	Theory	Experiment	Theory
Distance (Å)	Fe1-Fe2	2.5235(5)	2.574	2.5336(3)	2.576	2.5271(6)	2.578
	Fe2-Fe3	2.5210(5)	2.581	2.5290(3)	2.560	2.5068(6)	2.543
	$Fe1\text{-}CO_{terminal}$	1.753(3)	1.742	1.7544(18)	1.743	1.750(3)	1.743
	$Fe3\text{-}CO_{terminal}$	1.785(3)-1.805(3)	1.778 - 1.786	1.789(2)-1.803(2)	1.779 - 1.790	1.786(4)-1.794(4)	1.777-1.793
	$Fe1\text{-}CO_{bridging}$	2.314(3)	2.360	2.2719(17)	2.335	2.244(3)	2.330
	$Fe2\text{-}CO_{bridging}$	1.766(3)	1.754	1.7768(17)	1.757	1.783(3)	1.759
	Fe1-P1	2.2354(7)	2.278	2.2436(5)	2.279	2.2641(9)	2.283
	Fe1-P2	2.2559(7)	2.284	2.2533(5)	2.283	2.2417(8)	2.278
Angles (°)							
	Fe1-Fe2-Fe3	159.484(19)	159.68	160.464(13)	158.98	160.77(2)	158.00
	Fe2-C2-O2	157.5(2)	156.96	155.91(15)	156.53	155.7(2)	156.40
	Fe1-C2-O2	127.39(19)	127.18	127.62(13)	126.88	127.5(2)	126.83
	Fe2-C2-Fe1	75.06(9)	75.86	76.47(6)	76.57	76.79(12)	76.77
	Fe1-Fe2-C2	62.39(8)	62.78	60.59(5)	61.87	59.83(9)	61.62
	P1-Fe1-P2	87.45(3)	87.24	87.365(17)	87.3	87.04(3)	87.28

* L. Beaume, M. Clémancey, G. Blondin, C. Greco, F. Y. Pétillon, P. Schollhammer, J. Talarmin, *Organometallics* **2014**, *33* (22), 6290–6293.

Table S5. Crystallographic data of $[Fe_3(CO)_5(\kappa^2\text{-dppe})(\mu\text{-pdt}^{Et2})(\mu\text{-pdt})]_2.CH_2Cl_2$ (**$[2]_2.CH_2Cl_2$**) and $[Fe_3(CO)_5(\kappa^2\text{-dppe})(\mu\text{-pdt}^{Bn2})(\mu\text{-pdt})]$ (**3**)

	$[2]_2$, CH_2Cl_2	**3**
Empirical formula	$C_{83}H_{90}Cl_2Fe_6O_{10}P_4S_8$	$C_{51}H_{48}Fe_3O_5P_2S_4$
Formula weight	2033.91	1098.62
Temperature/ K	150(2)	150(2)
Wavelength/Å	0.71073	0.71073
Crystal system	Triclinic	Monoclinic
Space group	P -1	P 1 21/n 1
a (Å)	10.7156(2)	12.9425(4)
b (Å)	12.4815(2)	19.4734(5)
c (Å)	18.9827(4)	19.9676(6)
α (°)	73.604(2)	90
β (°)	89.158(2)	91.110(3)
γ (°)	66.590(2)	90
V (Å^3)	2221.40(7)	5031.6(3)
Z	1	4
ρ_{calcd} (Mg/mm^3)	1.520	1.450
μ (mm^{-1})	1.329	1.129
F(000)	1046	2264
Crystal size (mm)	0.55 x 0.40 x 0.17	0.27 x 0.19 x 0.04
Crystal color	Dark red	Dark red
Crystal shape	Planar truncated parallelepiped	Rectangular plate (-1 0 1) [0 1 0]
Range of θ (°)	3.45 to 30.51	3.30 to 26.37
Limiting indices	$-15 \le h \le 15$, $-17 \le k \le 17$, $-27 \le l \le 27$	$-14 \le h \le 16$, $-24 \le k \le 24$, $-24 \le l \le 24$
Reflections collected/unique	39408 / 13550	28957 / 10255
R_{int}	0.0362	0.0799
Completeness to θ = 26.37	99.8	99.7 %
Absorption correction	Semi-empirical from equivalents	Semi-empirical from equivalents
Max. / Min. Transmission	0.8056 / 0.5284	0.9562 / 0.7503
Refinement method	Full-matrix least-squares on F^2	Full-matrix least-squares on F^2
Data /Restraints /Parameters	13550 / 12 / 526	10255 / 0 / 586
R_1 [I>2σ(I)]	0.0350	0.0464
wR_2 [I>2σ(I)]	0.0857	0.1011
R_1 (all data)	0.0435	0.0706
wR_2 (all data)	0.0931	0.1159
Goodness of fit on F^2	1.090	1.035
$\Delta\rho_{max}$, $\Delta\rho_{min}$ [e.Å^{-3}]	0.587, -0.564	0.623, -0.483

Table S6. Natural Bond Orbital (NBO) and Mulliken analysis of atomic charges on Fe1, Fe2 and Fe3 atoms in **1** and **3**.

3	Fe1	Fe2	Fe3
Mulliken	-0.42	-0.26	-0.62
NBO	-0.18	+0.03	-0.20

1	Fe1	Fe2	Fe3
Mulliken	-0.40	-0.25	-0.62
NBO	-0.18	+0.01	-0.22

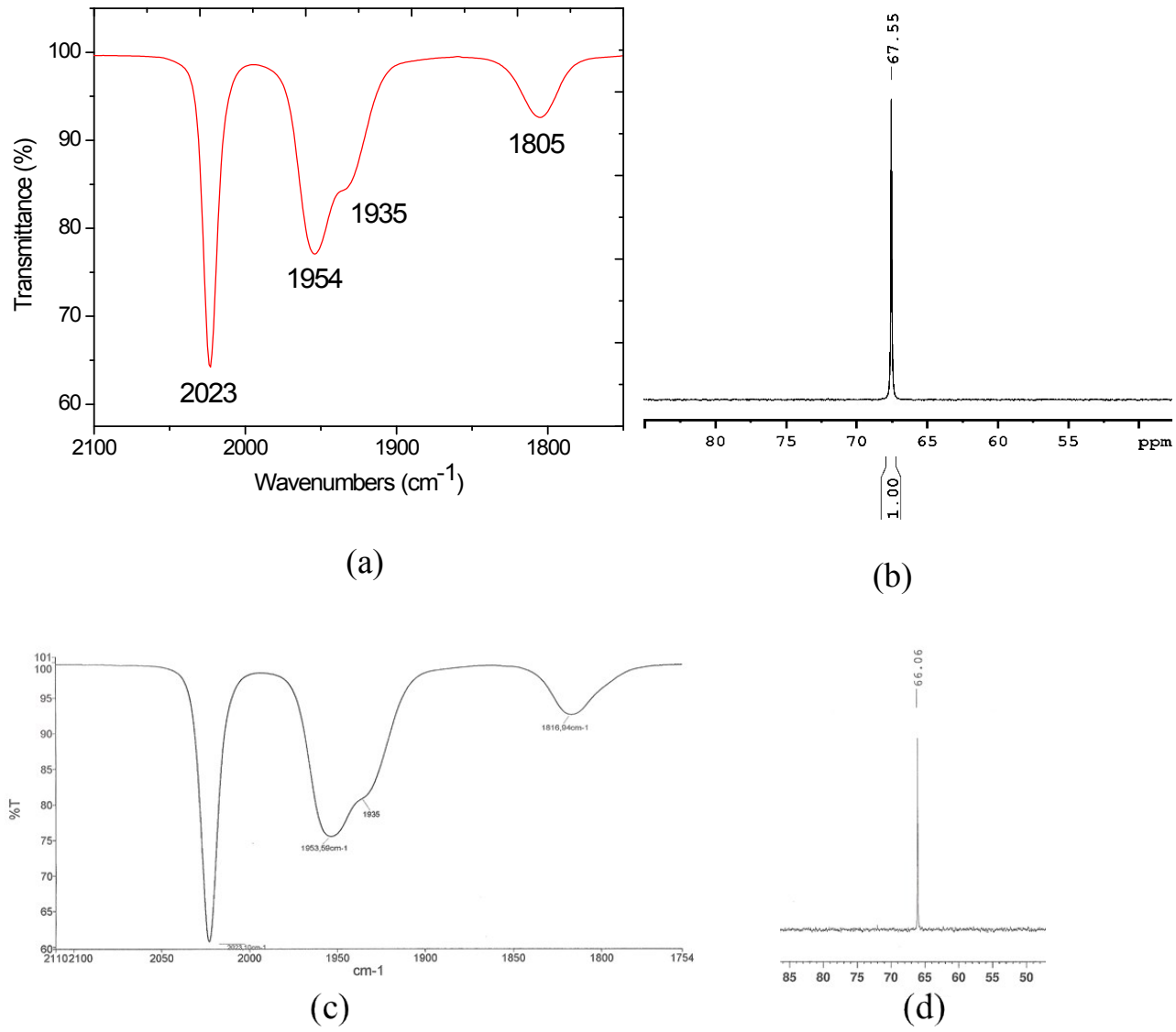

Figure S3. (a) IR (CH_2Cl_2) and (b) $^{31}P\{^1H\}$ NMR ($CDCl_3$) spectra of **2** at 25°C ; (c) IR (CH_2Cl_2) and (d) $^{31}P\{^1H\}$ NMR ($CDCl_3$) spectra of **3** at 25°C.

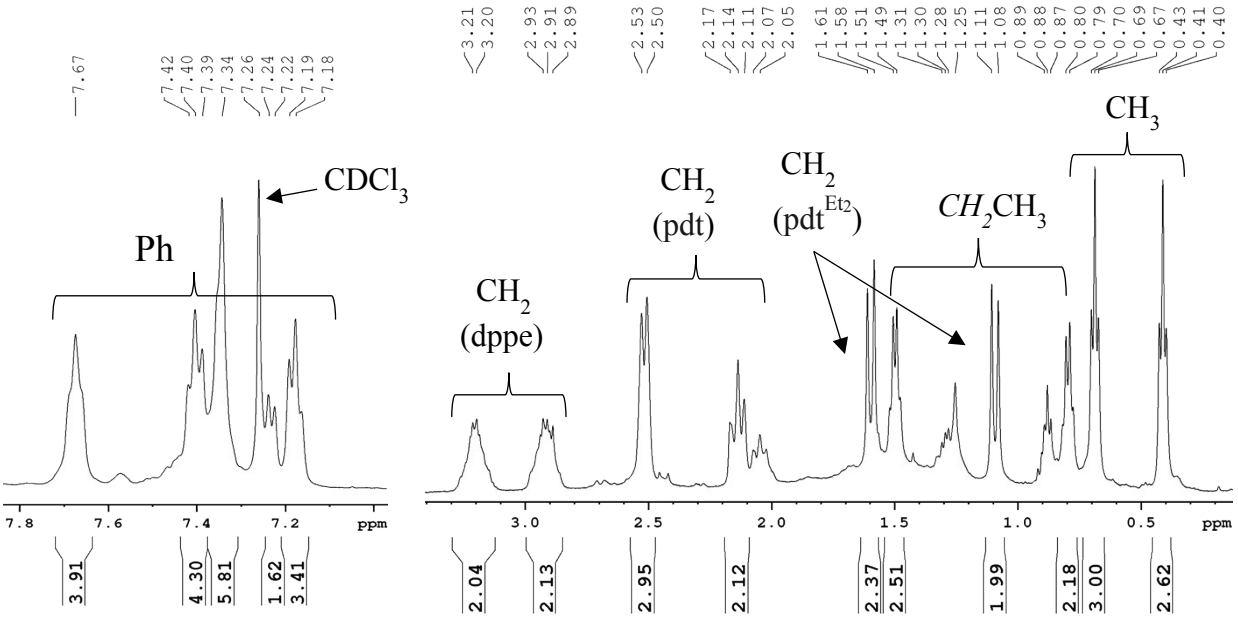

(a)

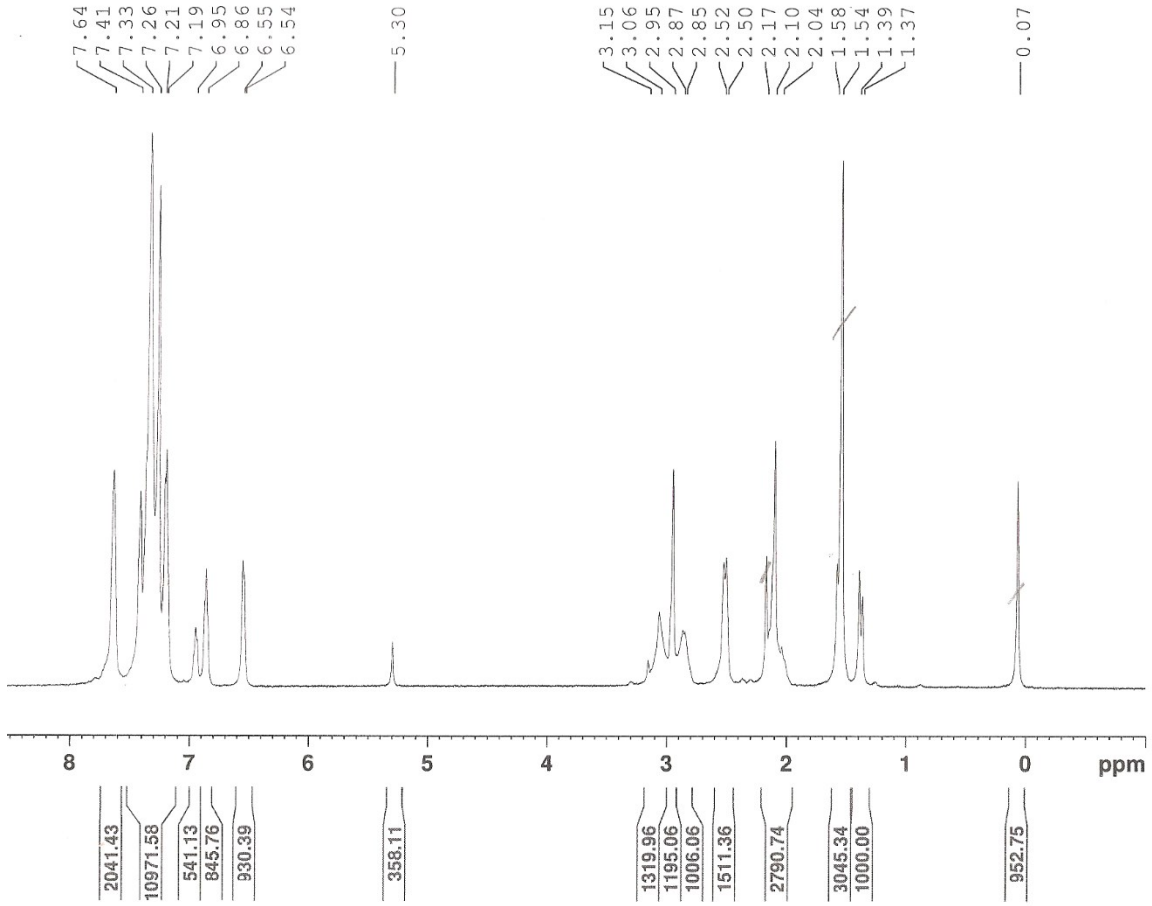

(b)

Figure S4. ^{1}H NMR spectrum of **2** (a) and **3** (b) in $CDCl_3$ at 25°C.

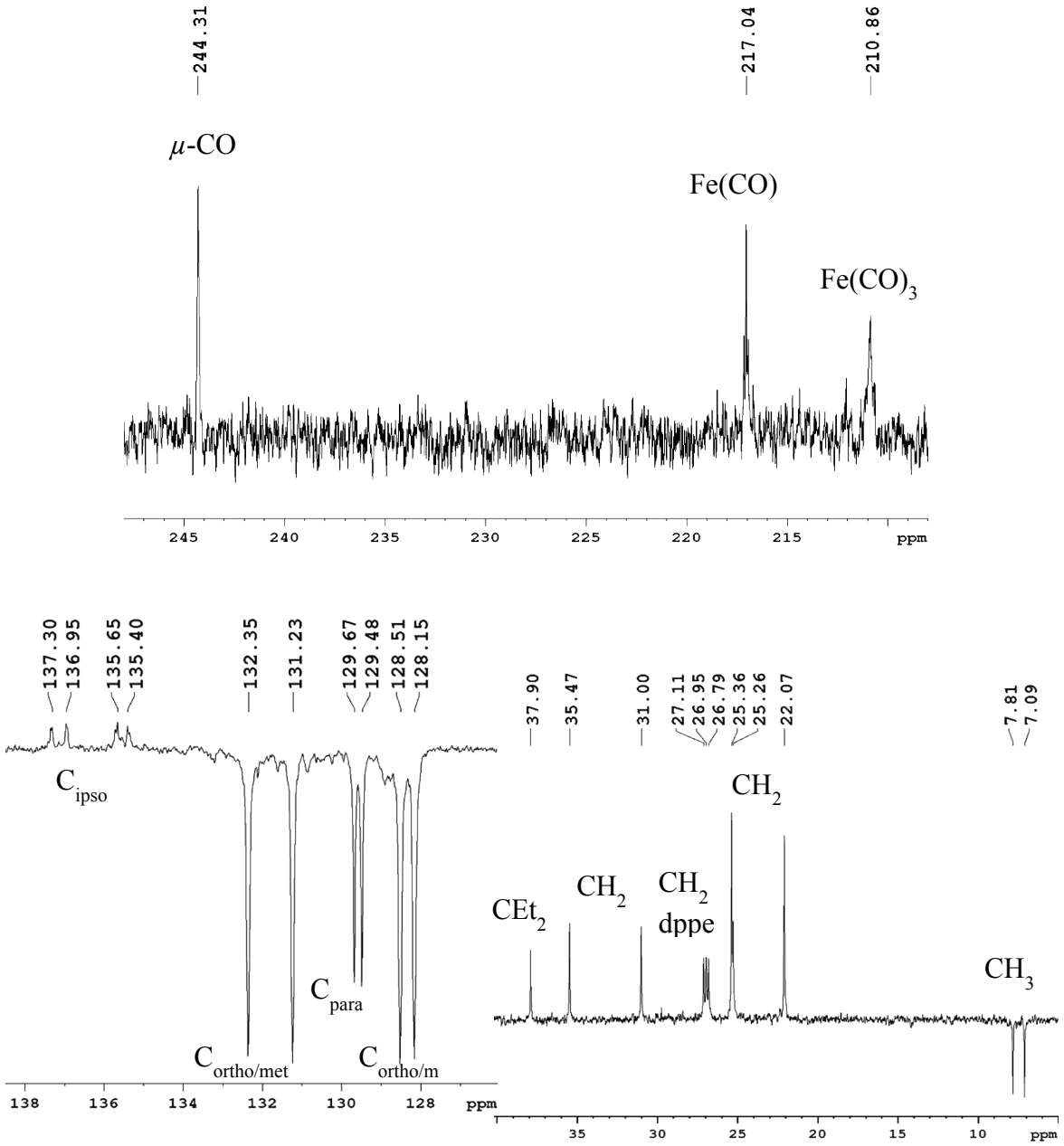

Figure S5. $^{13}C\{^{1}H\}$(Jmod) NMR spectrum of **2** in $CDCl_3$.

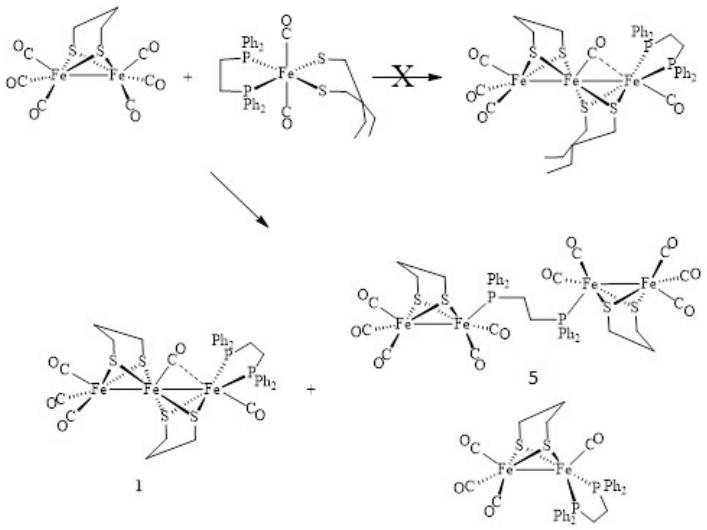

Scheme S1. Reaction between $[Fe_2(CO)_6(\mu\text{-pdt})]$ and $[Fe(CO)_2(\kappa^2\text{-dppe})(\kappa^2\text{-pdt}^{Et2})]$.

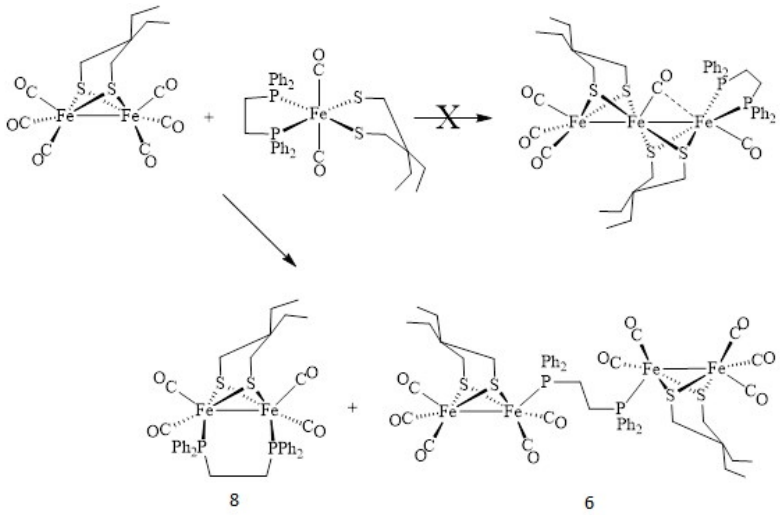

Scheme S2. Reaction between $[Fe_2(CO)_6(\mu\text{-pdt}^{Et2})]$ and $[Fe(CO)_2(\kappa^2\text{-dppe})(\kappa^2\text{-pdt}^{Et2})]$.

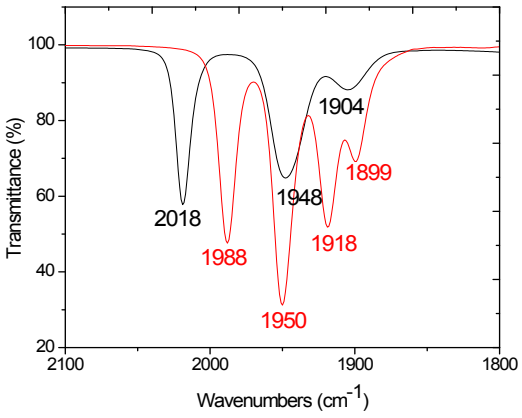

Figure S6. IR (CH_2Cl_2) spectra of $[Fe_2(CO)_4(\kappa^2\text{-dppe})(\mu\text{-pdt})]$ (black curve) and $[Fe_2(CO)_4(\mu\text{-dppe})(\mu\text{-pdt}^{Et2})]$ (**8**) (red curve).

Spectroscopic data for $[Fe_2(CO)_4(\mu\text{-dppe})(\mu\text{-pdt}^{Et_2})]$ (8)

IR (CH_2Cl_2, cm^{-1}) : $\bar{\upsilon}_{CO}$ = 1988 (s), 1950 (vs), 1918 (s), 1899 (m).

$^{31}P\text{-}\{^1H\}$ NMR ($CDCl_3$, ppm) : δ = 61.4 (s, dppe).

^1H NMR ($CDCl_3$, ppm) : δ = 7.65 – 7.38 (m, 20H, C_6H_5), 2.35 (m, 4H, dppe), 2.20 (m, CH_2, pdt^{Et2}), 1.62 (q, $^3J_{HH}$ = 7.2 Hz, 4H, CH_2CH_3), 0.82 (6H, t, $^3J_{HH}$ = 7.2 Hz, CH_3).

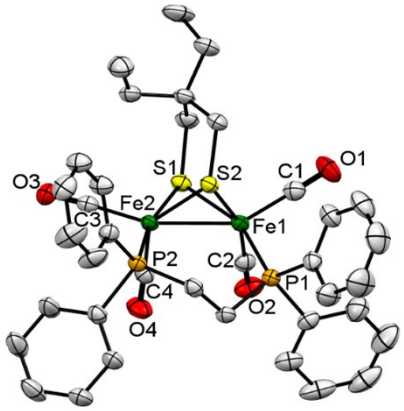

Figure S7. ORTEP view of $[Fe_2(CO)_4(\mu\text{-dppe})(\mu\text{-pdt}^{Et2})]$ (**8**)

Table S7. Selected distances and bond angles for **8**.

		8
Distance (Å)	Fe1-Fe2	2.5248(7)
	Fe1-S1	2.2660(10)
	Fe1-S2	2.2623(10)
	Fe2-S1	2.2546(9)
	Fe2-S2	2.2768(10)
	Fe1-P1	2.2221(10)
	Fe2-P2	2.2117(10)
Angles (°)	Fe1-Fe2-C3	155.53(12)
	Fe2-Fe1-C1	148.30(13)
	Fe1-S1-Fe2	67.91(5)
	Fe1-S2-Fe2	67.59(3)

Table S8. Crystallographic data of $[Fe_2(CO)_4(\mu\text{-dppe})(\mu\text{-pdt}^{Et2})]_2.2CH_2Cl_2$ (**8**)

	$[Fe_2(CO)_4(\mu\text{-dppe})(\mu\text{-pdt}^{Et2})]_2.2CH_2Cl_2$
Empirical formula	$C_{82}H_{94}Cl_4Fe_4O_8P_4S_4$
Formula weight	1824.89
Temperature/ K	170(2)
Wavelength/Å	0.71073
Crystal system	Triclinic
Space group	P-1
a (Å)	11.7315(4)
b (Å)	13.1271(4)
c (Å)	15.1143(5)
α (°)	97.110(3)
β (°)	110.969(3)
γ (°)	91.627(3)
V (Å^3)	2150.10(12)
Z	1
ρ_{calcd} (Mg/mm^3)	1.409
μ (mm^{-1})	1.009
F(000)	946
Crystal size (mm)	0.57 x 0.36 x 0.23
Crystal color	Red
Crystal shape	Block
Range of θ (°)	3.48 to 26.37
Limiting indices	$-10 \le h \le 14$, $-16 \le k \le 15$, $-18 \le l \le 12$
Reflections collected/unique	14652 / 8791
R_{int}	0.0473
Completeness to $\theta = 26.37$	99.6 %
Absorption correction	Semi-empirical from equivalents
Max. / Min. Transmission	0.8010 / 0.5969
Refinement method	Full-matrix least-squares on F^2
Data /Restraints /Parameters	8791 / 38 / 501
R_1 [I>2σ(I)]	0.0563
wR_2 [I>2σ(I)]	0.1589
R_1 (all data)	0.0694
wR_2 (all data)	0.1752
Goodness of fit on F^2	1.036
$\Delta\rho_{max}$, $\Delta\rho_{min}$ [e.Å^{-3}]	1.151, -1.136

Figure S8. HOMO-1, HOMO-2 and HOMO-3 of **1**.

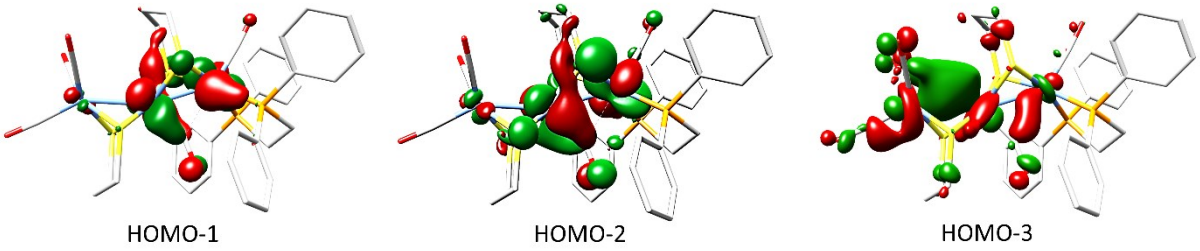

Table S9. Energy (eV) of the HOMO and LUMO orbitals of the complexes **1-4**, **9**

Complex	HOMO	LUMO
1	-4.353	-3.031
2	-4.329	-3.011
3	-4.338	-3.013
4	-4.381	-3.038
9	-4.555	-2.995

a)

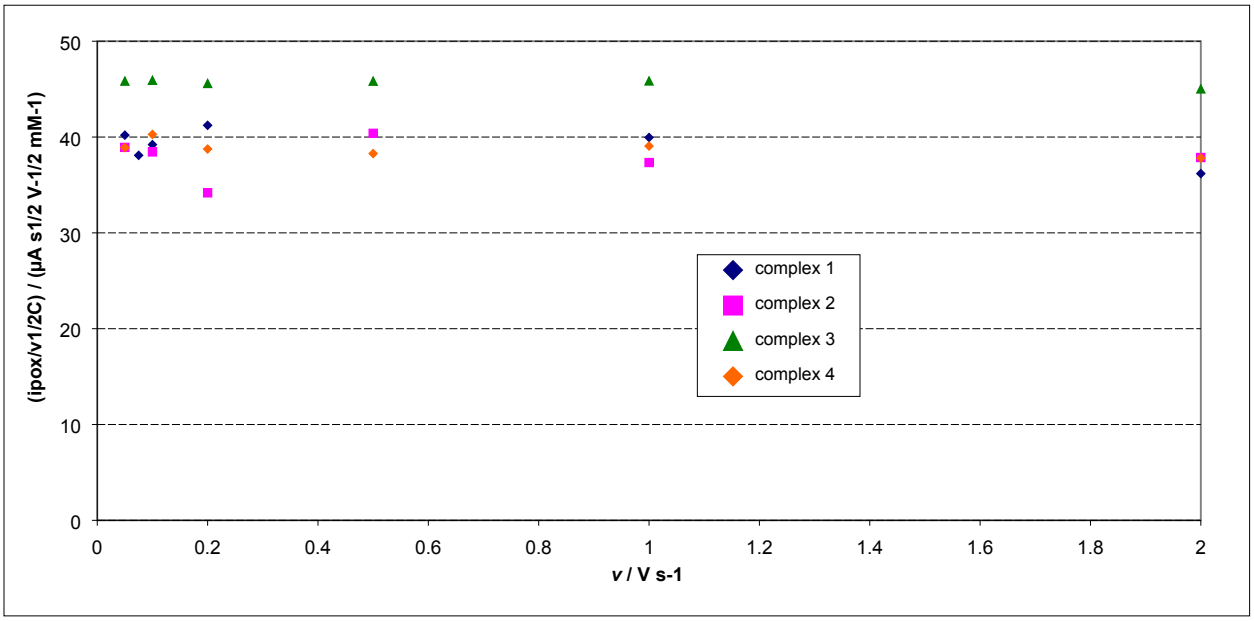

b)

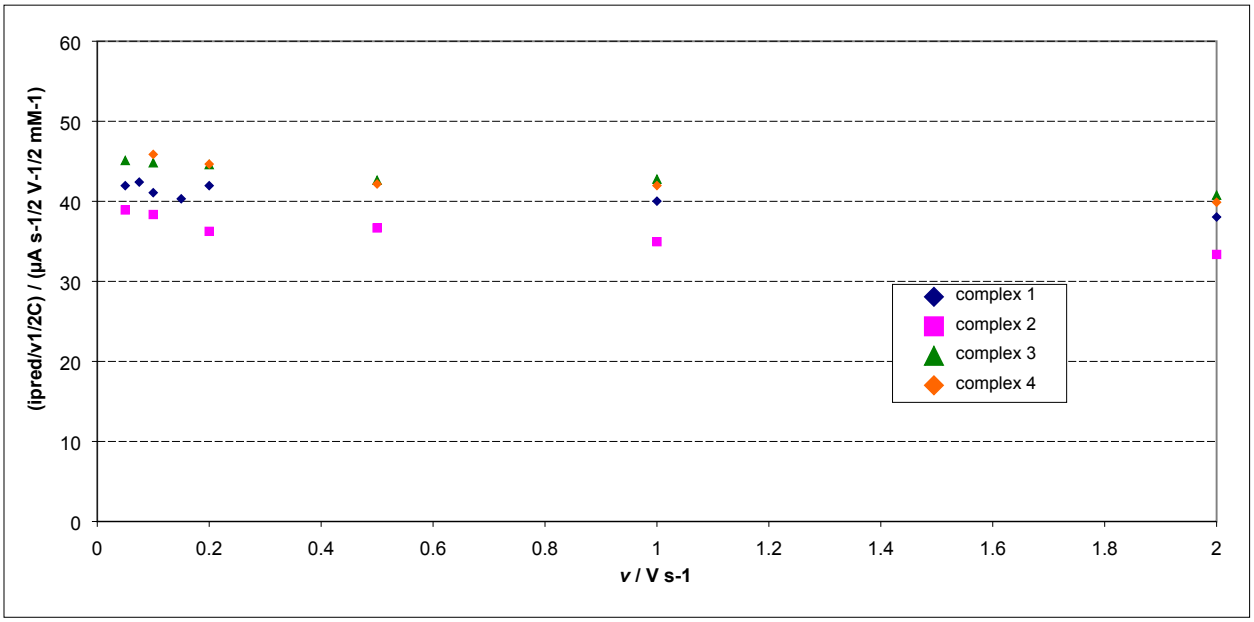

Figure S9. Scan rate dependence of the current function for the oxidation (a) and the reduction (b) of complexes **1-4** under inert atmosphere in CH_2Cl_2-$[NBu_4][PF_6]$ 0.2 M.

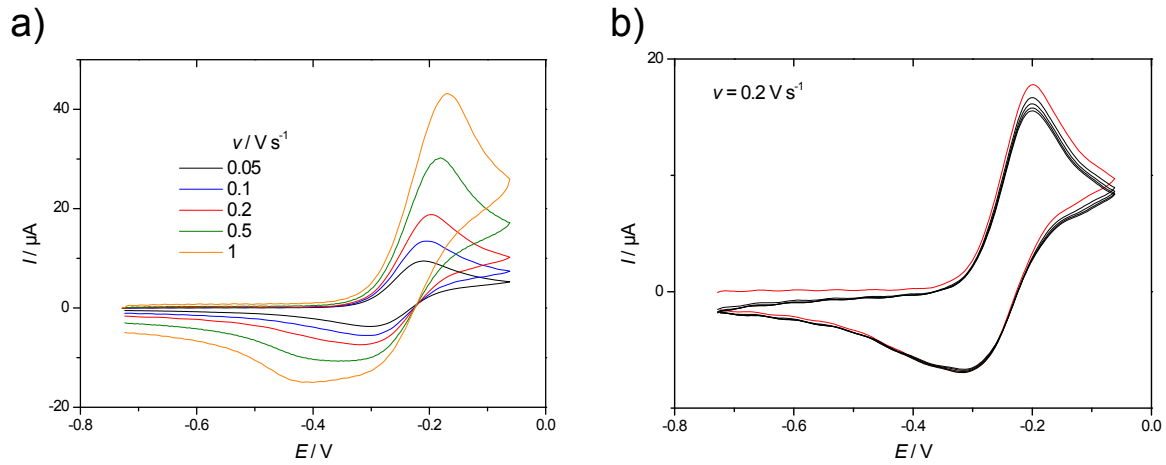

Figure S10. a) Oxidation of $[Fe_3(CO)_5(\kappa^2\text{-dppe})(\mu\text{-pdt}^{Bn2})(\mu\text{-pdt})]$ (**3**) (0.91 mM) under inert atmosphere in CH_2Cl_2-$[NBu_4][PF_6]$ 0.2 M at different scan rates. b) Successive cyclic voltammograms at 0.2 V s^{-1}.

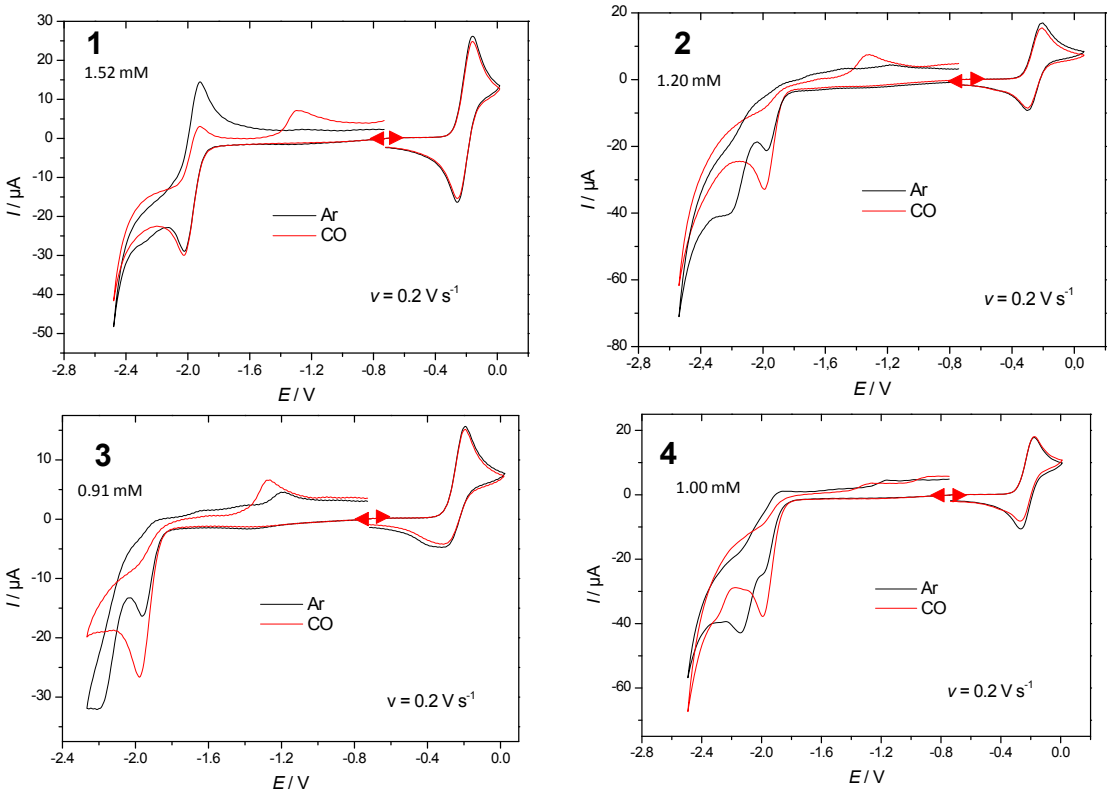

Figure S11. Comparison between cyclic voltammetry under Ar and CO for complexes **1**-**4** in CH_2Cl_2-$[NBu_4][PF_6]$ 0.2 M at $v = 0.2$ V s^{-1}.

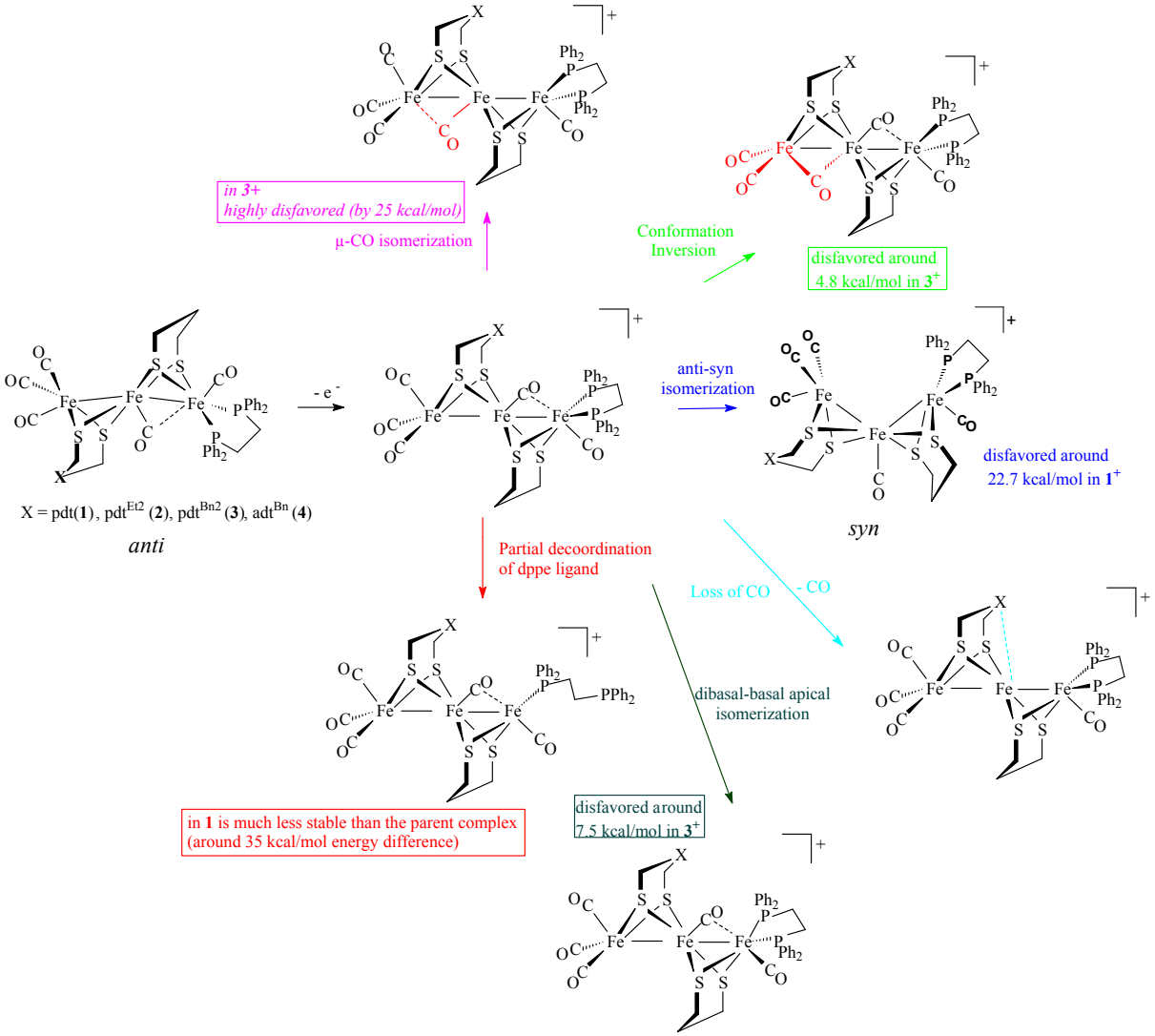

Scheme S3. Hypotheses for the reaction associated to the oxidation of triiron complexes

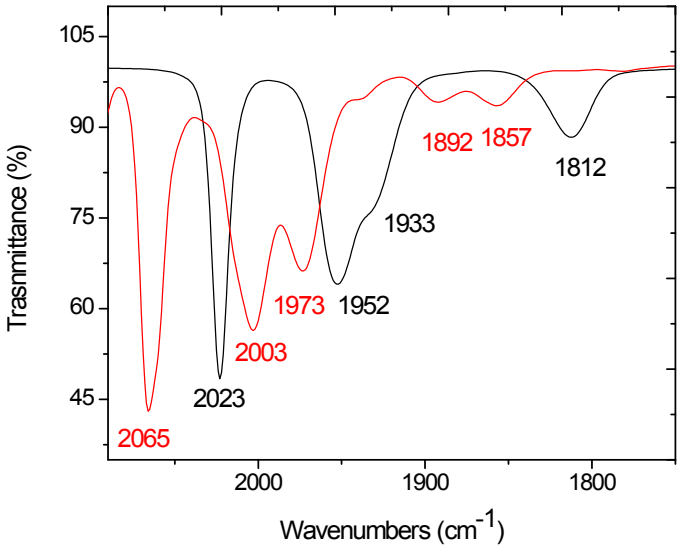

Figure S12. IR monitoring of the reaction of **1** in CH_2Cl_2 at -60°C with 1 equiv. of $[FeCp_2][BAr^F{}_4]$ (black curve: before; red curve: after addition of $[FeCp_2][BAr^F{}_4]$).

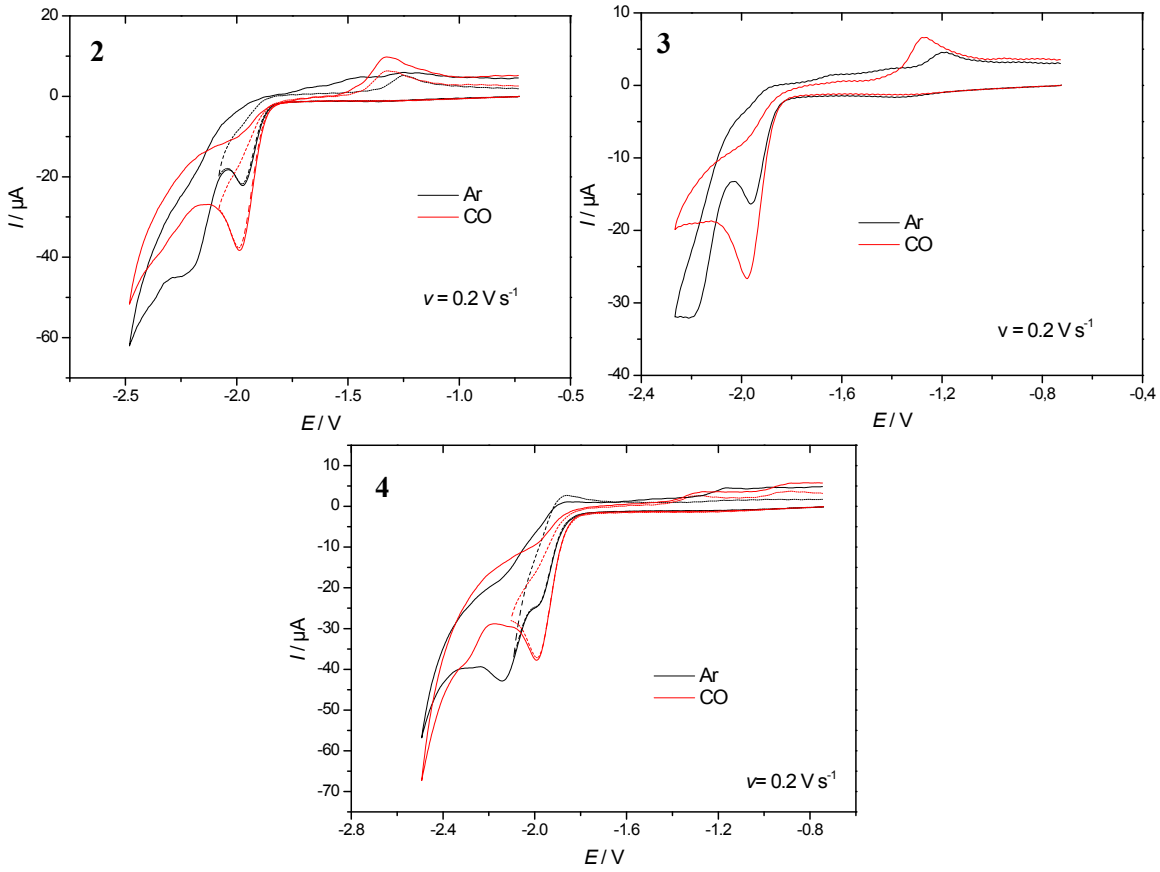

Figure S13. Reduction of **2** (1.20 mM), **3** (0.91mM) and **4** (1.50 mM) in CH_2Cl_2-$[NBu_4][PF_6]$ 0.2 M at 0.2 V s^{-1} under Ar and CO.

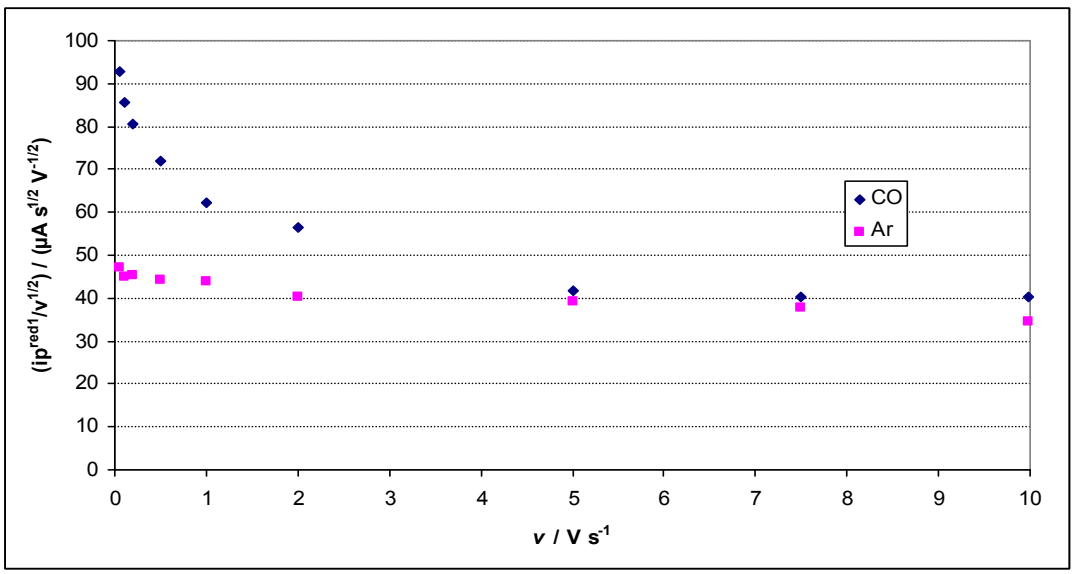

Figure S14. Scan rate dependence of the reduction current functions ($i_p^{red}/ v^{1/2}$) for the reduction of **2** (1.20 mM) in CH_2Cl_2-$[NBu_4][PF_6]$ 0.2 M under Ar and CO.

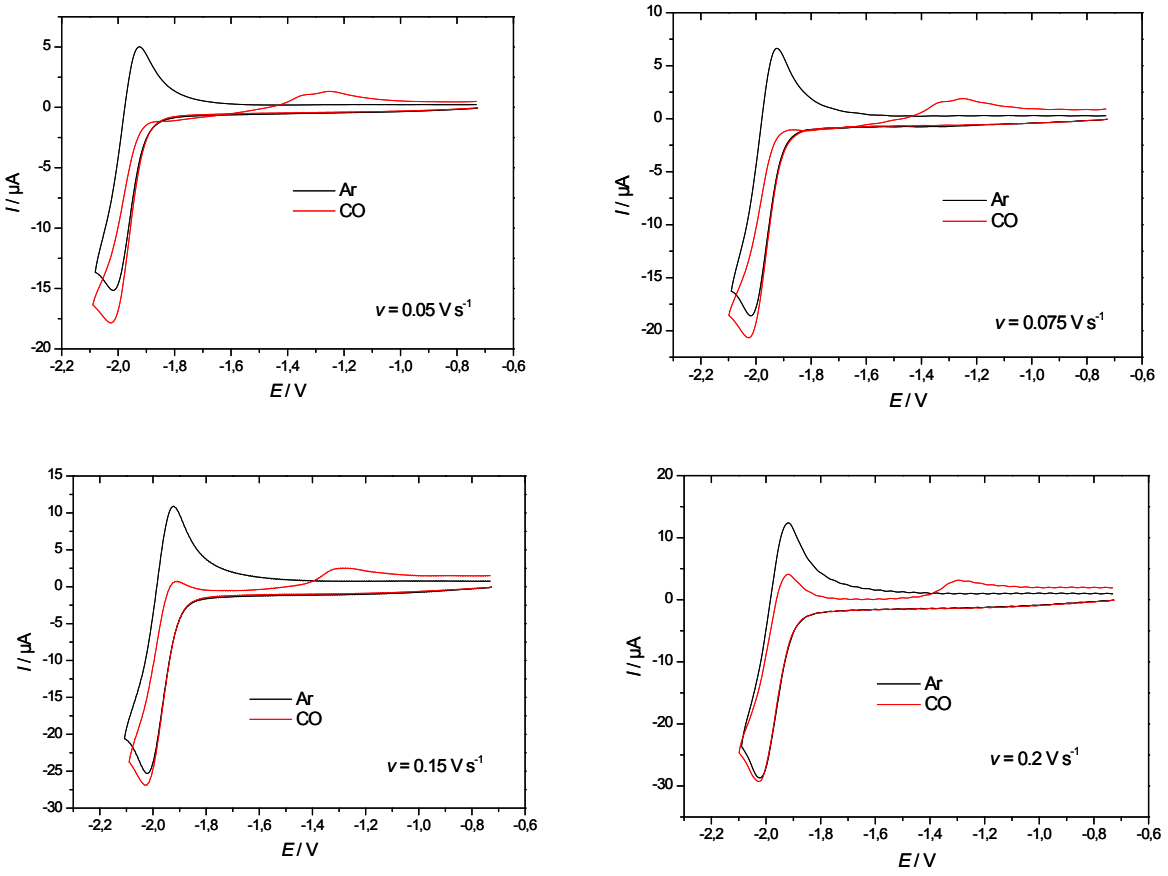

Figure S15. Reduction of $[Fe_3(CO)_5(\kappa^2\text{-dppe})(\mu\text{-pdt})_2]$ (**1**) (1.52 mM) under Ar and CO in CH_2Cl_2-$[NBu_4][PF_6]$ 0.2 M at slow scan rates.

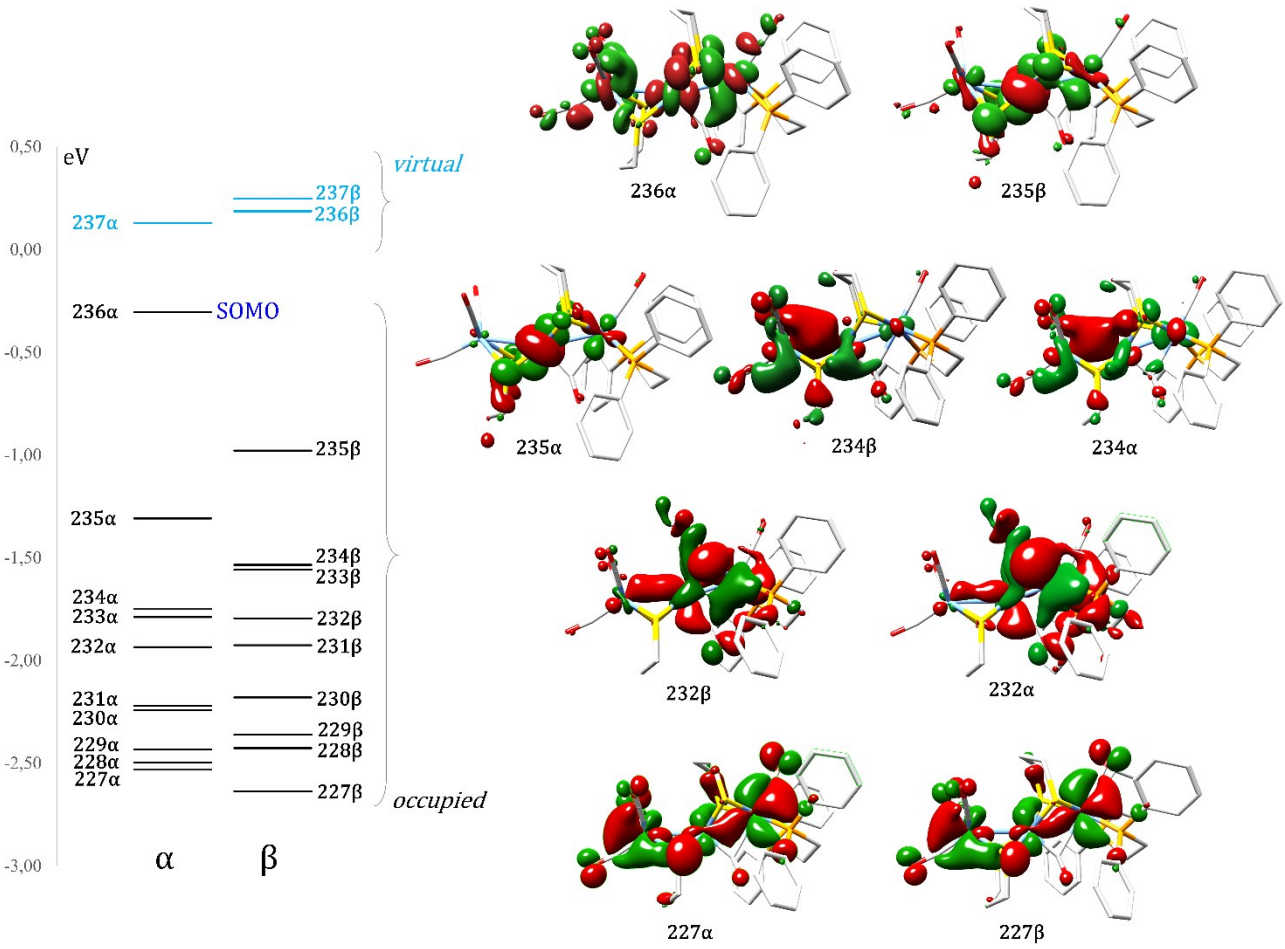

Figure S16. MO's energy diagram (left). Representation of MO discussed in the text (right).

Inspection of molecular orbitals shows that there are several orbitals with FeFe binding character : those in which this is evident are the following: 234α, 234β, 232α, 232β for the FeFe pair including Fe2 and Fe3; 227α and 227β for the pair formed by the central iron atom and by the diphosphine-bound to the iron Fe1. As far as the rationalization of the computed spin populations at iron atoms is concerned, visual inspection of the three higher energy, singly occupied orbitals can justify in a qualitative way the delocalized picture coming from population analysis. In fact, the SOMO (i.e. 236α), which has antibonding character relative to iron atoms, shows that there is alpha density distributed over the three Fe atoms, with a slight preponderance at the iron Fe2. In any case, to understand why the spin population value is significantly higher on the latter Fe centre, one has to look also at the two singly occupied orbitals just below the SOMO, i.e. 235β and 235α.

These two orbitals are very similar to each other in correspondence of the central iron atom, and hence they have little overall effect in determining the spin population of the latter iron centre. However, the 235β orbital has significant contributions from the atomic orbitals

centered at Fe1, as well as from those centered on Fe3. Since the latter orbital is occupied by a β-spin electron, it contributes to lower the overall spin population value of the latter two irons. As far as the "building-up" of the 235α orbital is concerned, the atomic orbitals centered on Fe3 contribute in a negligible way, whereas the atomic orbitals of the diphosphine-bound Fe1 contribute in a significant way. However, the latter contribution is less pronounced than the one of atomic orbitals centered on Fe1, as far as the building up of 235β orbital is concerned. Therefore, orbitals 235β and 235α together add a significant amount of beta density on Fe3, reducing its spin population to a value that is close to be negligible (0.12). Actually, orbitals 235β and 235α have an overall effect of adding beta density also at the level of Fe1, although to a lesser extent than in the previous case. Such observation – together with the previous ones on the negligible effects of 235β and 235α orbitals in determining the spin population of Fe2 – makes sense of the fact that the spin population value of the latter iron atom is higher than that of Fe3, and lower than that of Fe2. Obviously, this discussion is qualitative, because it ignores the contributions due to all the differences between pairs of alpha and beta orbitals placed at deeper energies with respect to 235α. These differences actually exist, but based on visual inspection it is clear that around the Fe atoms such differences are generally small or very small for all those orbitals. The latter consideration further justifies our choice of focusing on SOMO, 235β and 235α to get a rationalization of the computed spin densities at the Fe ions.

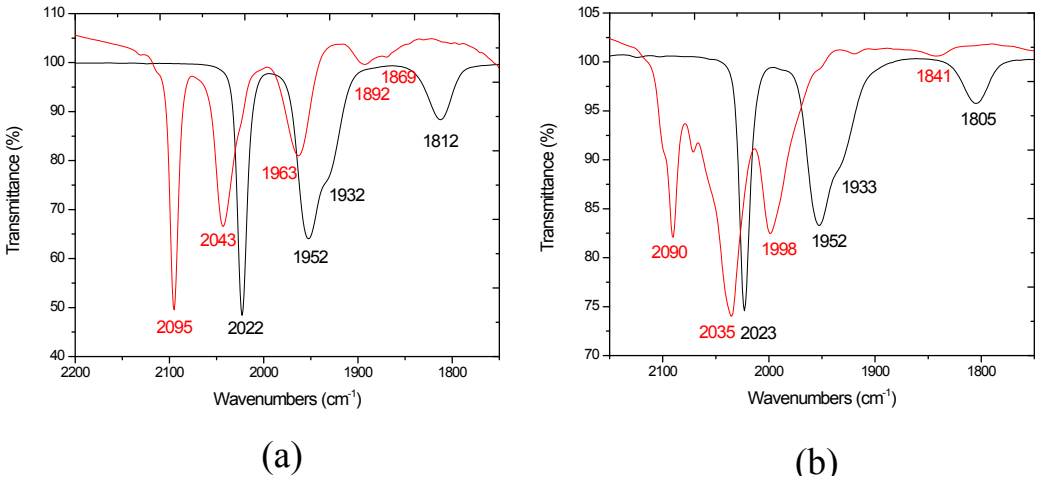

Figure S17. IR monitoring of the reaction of **1** (a), **2** (b) with 2 equiv. of $HBF_4.Et_2O$ at - 80°C in CH_2Cl_2 (black curve: before; red curve: after addition of acid).

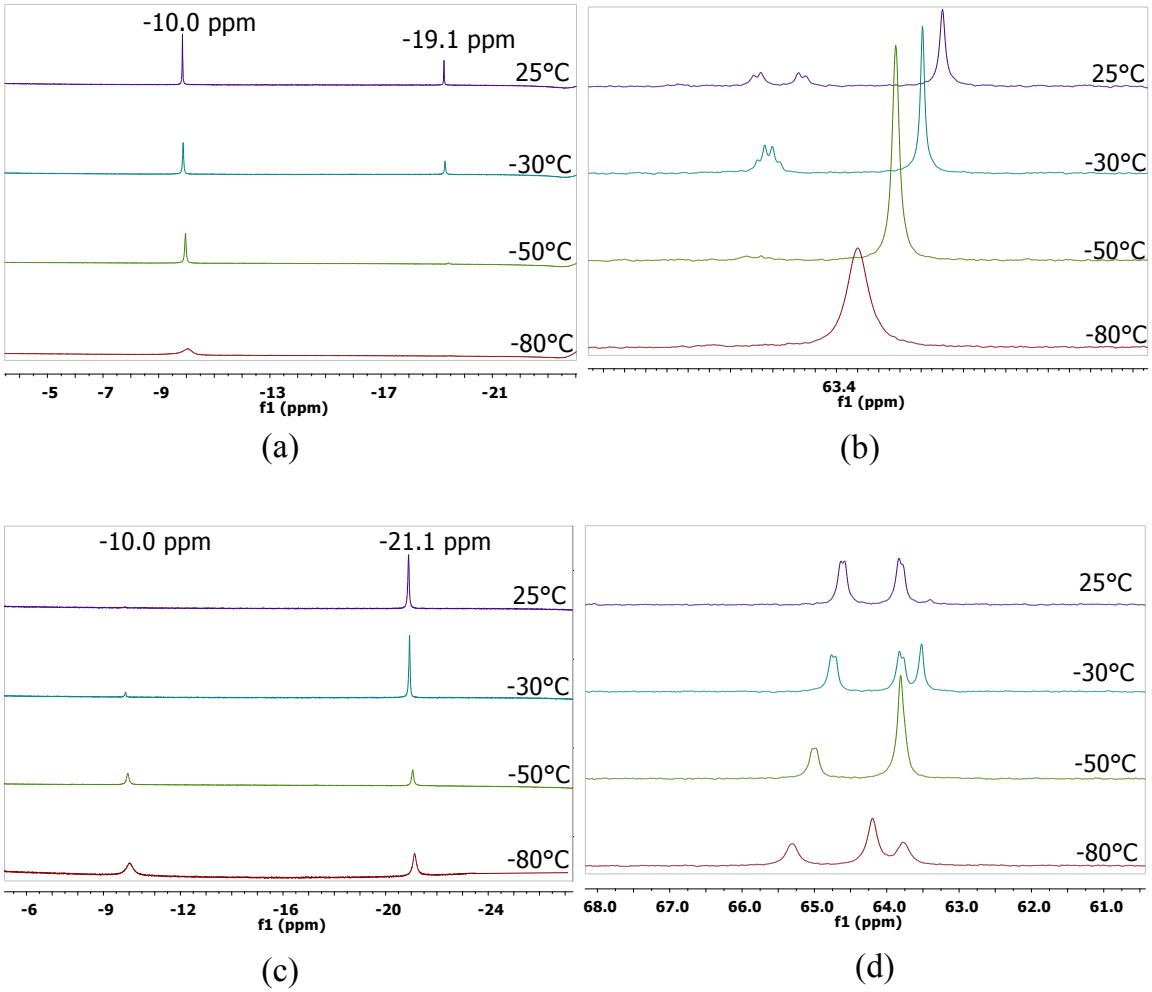

Figure S18. ^{1}H (a), (c) and $^{31}P\{^{1}H\}$ (b), (d) NMR monitoring, at variable temperature, of the reaction of **1** (a), (b), **2** (c),(d) in the presence of 2 equiv. $HBF_4.Et_2O$ in CD_2Cl_2.

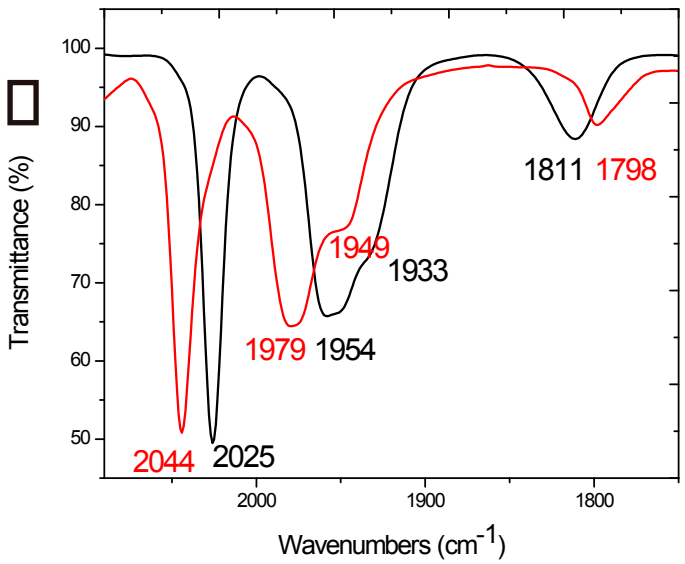

Figure S19. IR monitoring of the reaction of **4** with $HBF_4.Et_2O$ (2 equiv) at 25°C in CH_2Cl_2 (black curve: before; red curve: after addition of acid).

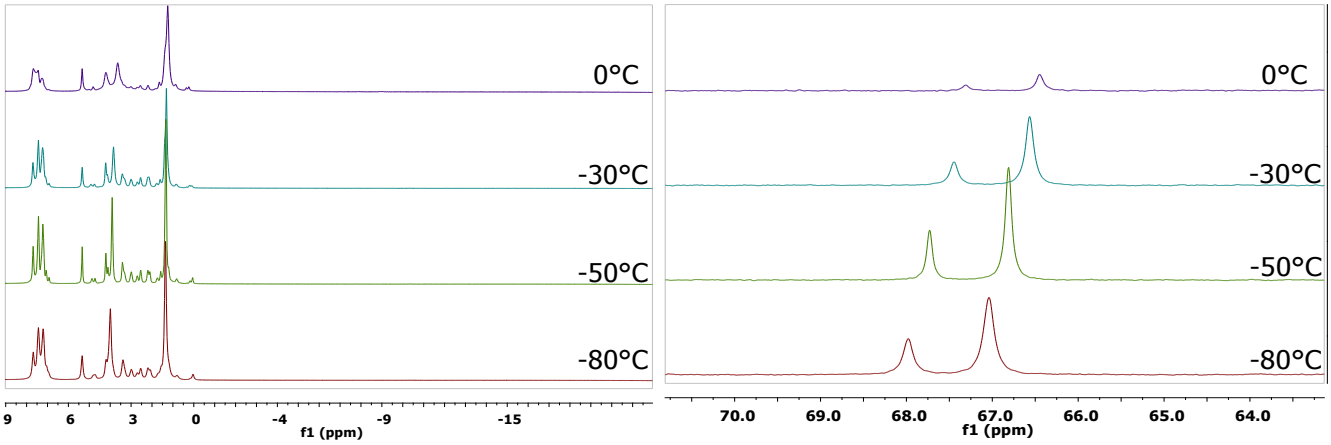

(a) (b)

Figure S20. ^{1}H (a) and $^{31}P\{^{1}H\}$ (b) NMR monitoring, at variable temperature, of the reaction of **4** in the presence of 2 equiv. of $HBF_4.Et_2O$ in CD_2Cl_2.

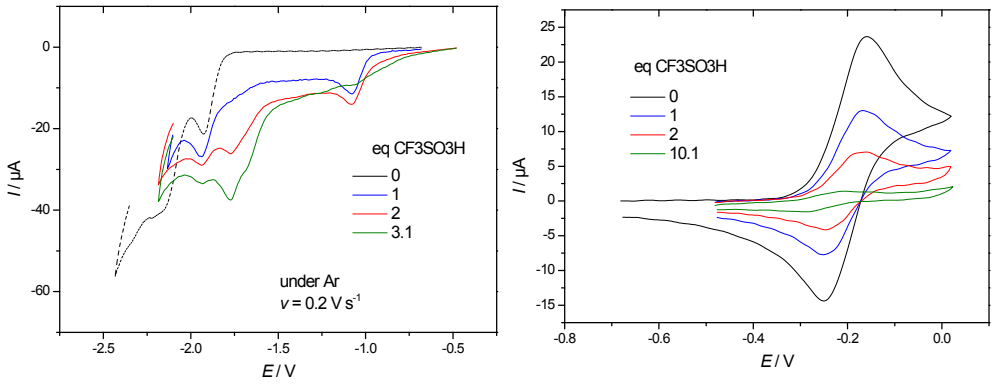

Figure S21. Cyclic voltammetry of $[Fe_3(CO)_5(\kappa^2\text{-dppe})(\mu\text{-pdt}^{Et2})(\mu\text{-pdt})]$ (**2**) (C = 1.20 mM) in presence of CF_3SO_3H in CH_2Cl_2-$[NBu_4][PF_6]$ 0.2 M at v = 0.2 V s^{-1} under Ar .

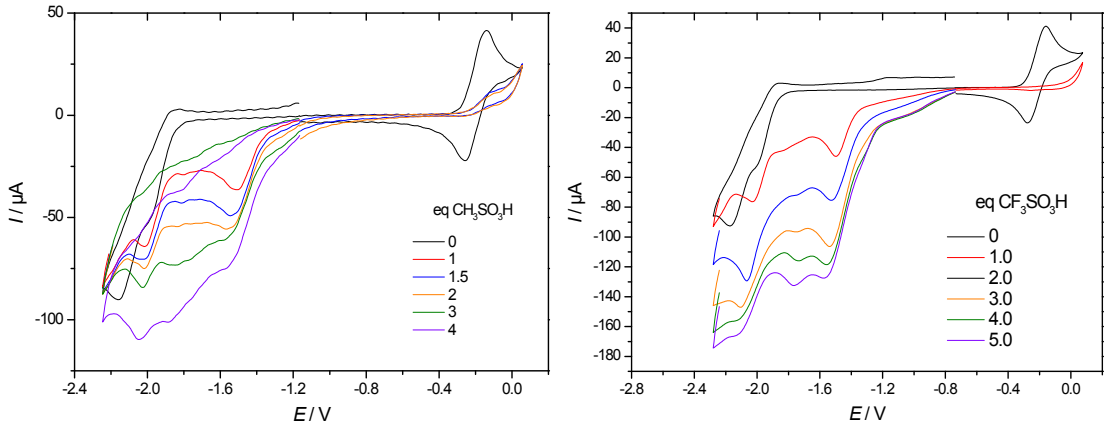

Figure S22. Cyclic voltammetry of **4** (2.2 mM) in presence of CH_3SO_3H (left) and CF_3SO_3H (right) in CH_2Cl_2-$[NBu_4][PF_6]$ 0.2 M.